Arab J Geosci (2016) 9: 692
DOI 10.1007/s12517-016-2685-2

ORIGINAL PAPER

# Relationships among volcanic and hydrothermal activity and faults from the Shunnan 3-D well zone in the Tadong Area (Tarim Basin, China)

**Li KunBai[1] · Lv HaiTao[2] · Pu RenHai[1] · Cao ZiCheng[2]**

Received: 13 March 2016 / Accepted: 19 September 2016 / Published online: 3 November 2016


**Abstract** Tarim Basin distributed widely two stages of Permian volcanic rocks. However, the location and timing of these rocks pinching out and the relationship between Ordovician carbonate hydrothermal reservoirs and fault activity remain unclear. The Shunnan (Shunnan here in after referred to as SN) 1 3-D well zone in the eastern Tarim Basin contains volcanic rocks, and the Ordovician layer contains a hydrothermal reservoir. This paper describes the lithology, stage, volcanic rock distribution, crater position and deposition pinch-out line of volcanic rocks based on drilling and 3-D seismic data. The Permian strata in the well zone contain only one stage of Kupkuciman Formation basalt and tuff, the Kaipeleicike Formation contains terrigenous clastic rock and the adjacent volcanic rocks of wells SN2 and GL (Gulong here in after referred to as GL) 2 exhibit an absence of deposition. Although the craters are distributed on both sides of the NNW faults that cross well SN4, their positions are also controlled by the intersection of earlier NEE and NW faults and later NNE faults. Furthermore, the Ordovician strata in the SN1 well zone developed abundant tubular high-amplitude anomalies and tabular high-amplitude anomalies via hydrothermal corrosion, and the anomaly distributions are similar to the positions of the craters, which are controlled by the intersection of multi-group faults and the density of the faults.

✉ Pu RenHai
purenhai@126.com

[1] State Key Laboratory of Continental Dynamics, Department of Geology, Northwest University, Xi'an 710069, China

[2] Northwest Oilfield Branch Company of SINOPEC, Urumqi 830011, China

**Keywords** Tarim Basin · Volcanic rock pinching · Volcano stage · Crater · Fault · Hydrothermal reservoir

## Introduction

The Tarim large igneous province (TLIP) in northwestern China was formed in the Early Permian (Fig. 1a). The TLIP includes large volumes of flood basalts and mafic-ultramafic intrusions (Mahoney and Coffin, 1997; Pirajno, 2000; Derek, 2003; Ernst and Buchan, 2003). The formation of the TLIP is related to that of the ~260-Ma Emeishan LIP in southwest China (Chung and Jahn, 1995; Xu et al. 2001; Zhou et al. 2002) and the ~250-Ma Siberian Traps in Russia (Campbell et al. 1992; Arndt et al. 1998; Reichow et al. 2009). Elucidating the process of Permian magmatism is crucial for understanding its relationship with the tectonic evolution and the Ordovician hydrothermal reservoirs of the survey area.

The SN 3-D seismic survey is located in the central part of the Tarim Basin at the eastern part of the Tazhong uplift (Fig. 1b). Well SN4 in the survey has produced commercial gas from Ordovician carbonate reservoirs. These hydrothermal reservoirs are related to the faults and volcanic activity. As a result, insights into the Permian volcanic rock distribution and volcanic stages are useful for understanding Ordovician hydrothermal reservoirs. The Tarim Basin has widely distributed volcanic rocks. Yang (2005) drew a map of all the basic and acid volcanic rocks in the basin (Fig. 1c). Two sets of volcanic rocks pinch out in the eastern Tarim Basin, and it is unclear whether this hiatus resulted from erosion or the lack of deposition. Although the Permian volcanic rocks in the Tarim Basin have been intensively studied, most methods used to determine the composition, date and source of the rocks involve field investigations and geochemical experiments. In addition, Keping and Bachu have been the main

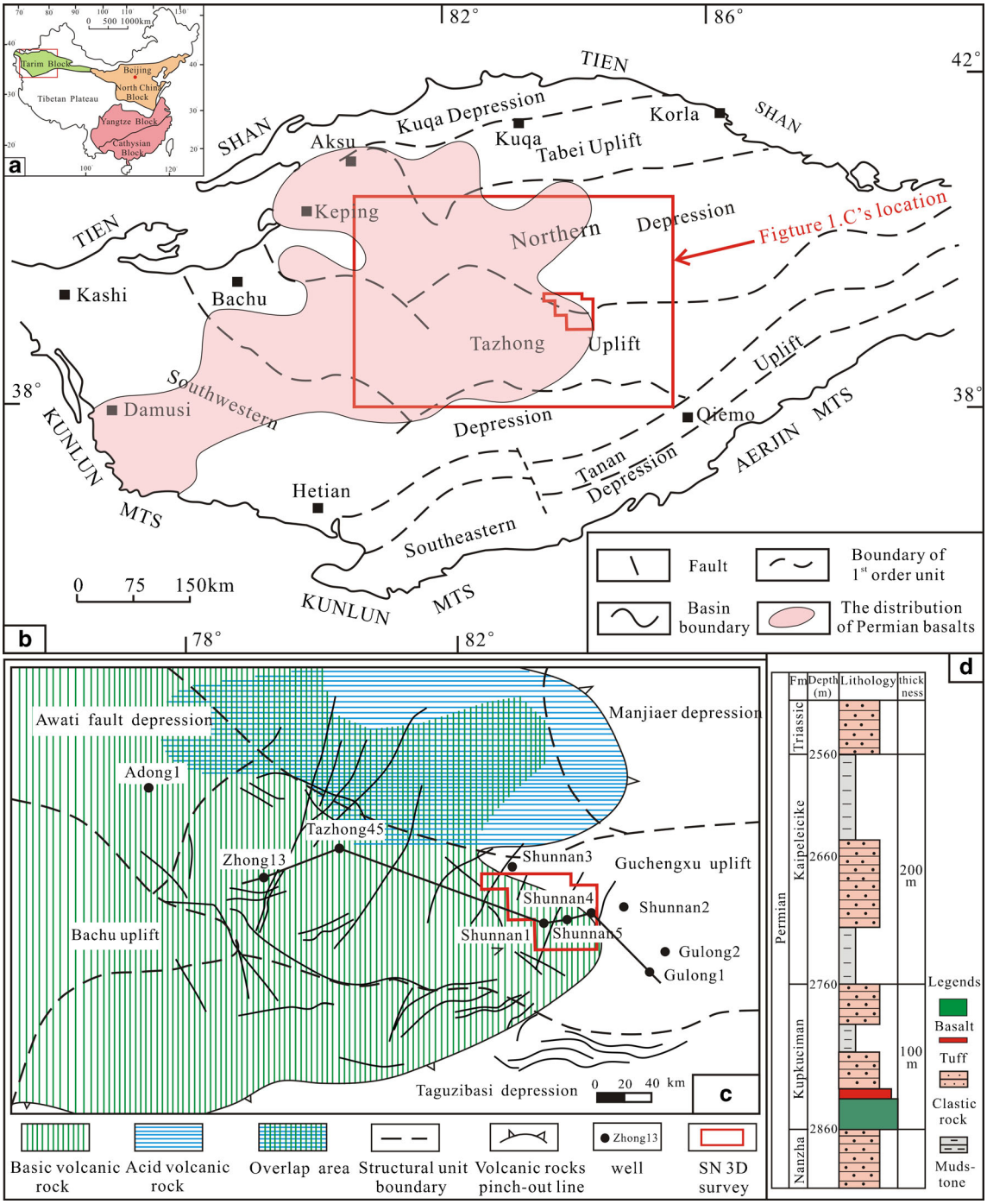


**Fig. 1** **a** The location of the Tarim Basin in China. **b** The distribution of the basic basalt rocks in the Tarim Basin. **c** The location of the SN 3-D seismic survey and distribution of igneous rocks around the survey (Yang et al. 2005). **d** Generalized Permian stratigraphy in the SN 3-D survey (Pu et al. 2011)

study areas (Li et al. 2014; Xu et al. 2014; Zhou et al. 2009). However, the distribution, stage, lithology and pinch-out line of volcanic rocks in the SN area remain unclear. Thus, gaps exist in vital knowledge for the investigation of hydrothermal activity.

Based on drilling and 3-D seismic data, this paper analyses the lithology, distribution and stage of the volcanic rocks, the position of the craters and the pinch-out type of the volcanic rocks by the methods of 3-D seismic horizon tracking, post-stack inversion, attribute extraction, volcanic rocks logging crossplot and horizontal well tie contrast to reveal the relationships of these parameters with faults and hydrothermal activity and to obtain useful insights into the formation of hydrothermal reservoirs and hydrocarbon exploration in Shunnan area.

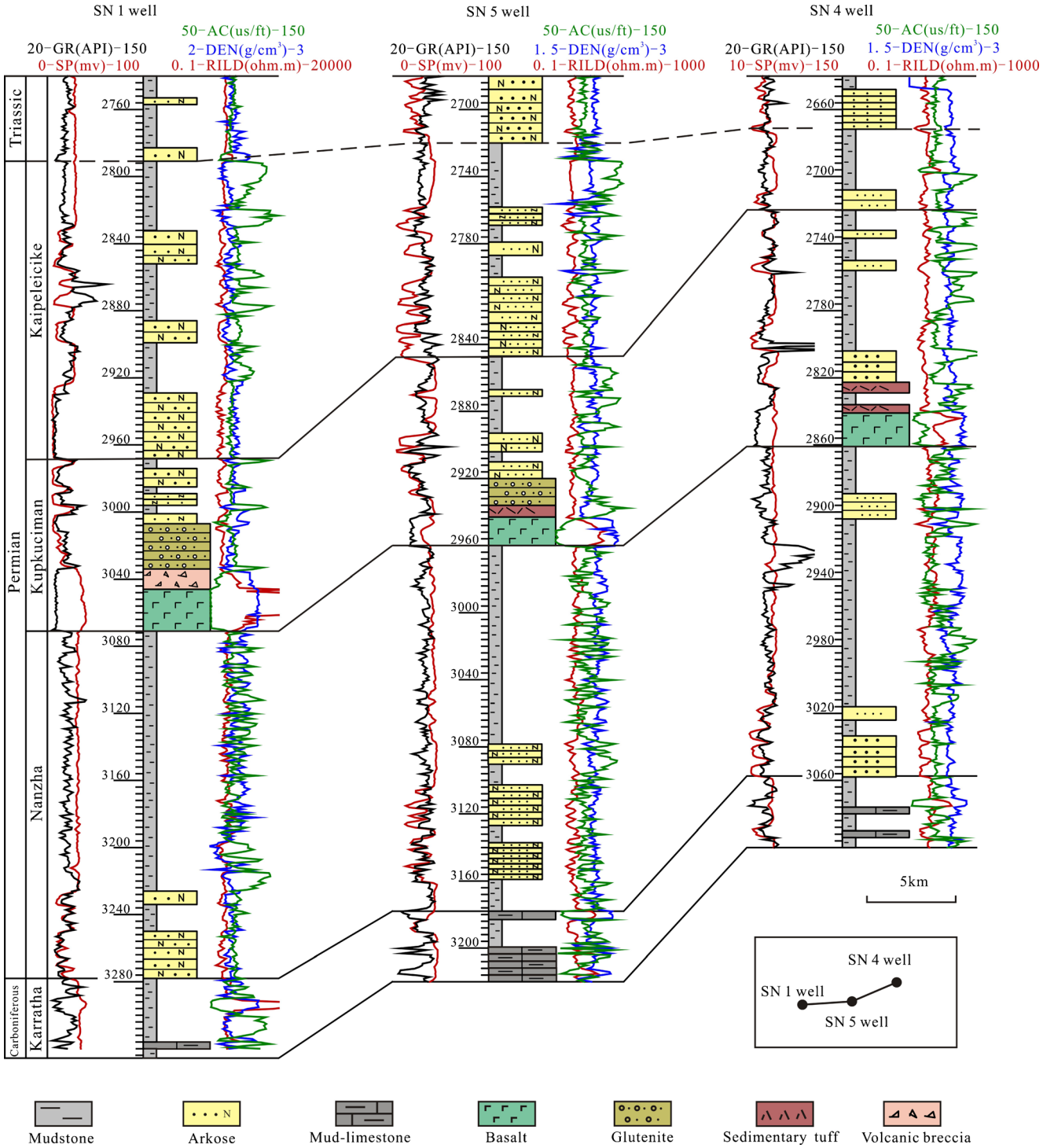


**Fig. 2** The Permian stratigraphic cross-sections of wells SN1, SN5 and SN4 in the SN3-D survey. The Permian Kupkuciman Formation developed one stage of basalt, whereas the Kaipeleicike Formation is composed of terrigenous clastic rock only. See Fig. 1 for the well locations

## Geological background

The Tarim Basin is located in the south of the Xinjiang Uygur Autonomous Region in northwest China (Fig. 1a). It is the largest inland basin in China, covering approximately 530,000 km$^2$. The basin is bounded by the Tianshan orogenic belts to the north and west and the Kunlun and Aerjin orogenic belts to the south (Fig. 1b). The Tarim Basin is composed of a Precambrian crystalline basement and a thick Palaeozoic-Mesozoic-Cenozoic sedimentary cover (Long et al. 2011).

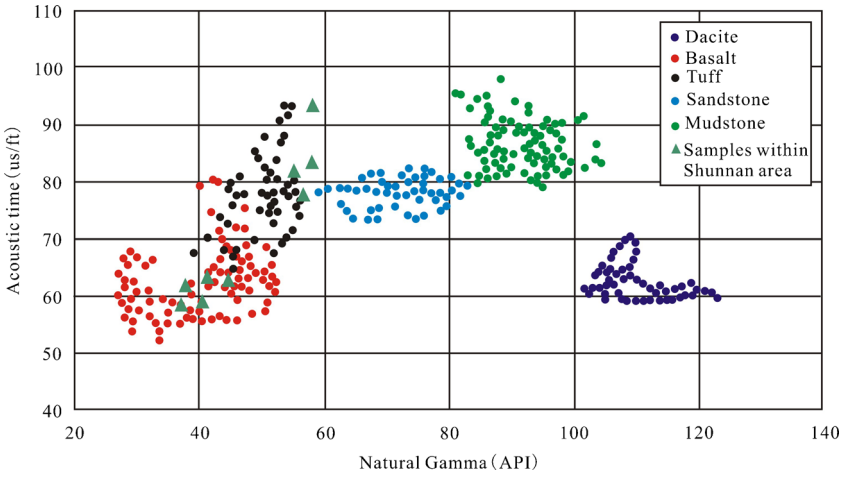


**Fig. 3** The logging crossplot of volcanic rocks in the Tahe and SN areas (modified by Luo et al. 2006). Some of the samples within the 3-D survey exhibit low natural gamma (approximately 40 API) and low AC (57–65 μs/ft) and are basalt. In contrast, others within the 3-D survey exhibit high natural gamma (57–60 API) and high AC (78–92 μs/ft) and are tuff

Several major periods of tectono-hydrothermal activity have been identified in the Tarim Basin, and the four most important are Neoproterozoic (774–673 Ma), Ordovician (460–484 Ma), Permian (264–282 Ma) and Cretaceous (~100 Ma). In addition, the Permian magmatism is closely related to the formation of the TLIP.

According to the increasingly rich set of seismic and drilling data, large volumes of both mafic and felsic igneous rocks were emplaced in the Tarim block during the Permian. The mafic series are dominated by basalt, andesitic basalt, diabase and ultramafic rocks, whereas the felsic bodies are dominated by syenite, rhyolite and dacite (Yang et al. 1997; Chen et al. 2006; Li et al. 2014; Wu et al. 2012a; Yang et al. 1996; Chen et al. 2010; Xu et al. 2014). The Tarim LIP consists predominantly of flood basalts that occupy a large area in the western and southwestern parts of the Tarim Basin. The Permian flood basalts in the Tarim Basin thicken from southwest to northeast, and the two most important areas of exposure are the Keping and Damusi regions. The full extent of volcanic rocks in the basin remains unknown because of the deep Palaeozoic to Cenozoic sedimentary cover, and some parts of the volcanic rocks occur in the subsurface (covered by the Taklamagan desert) (Xu et al. 2014). However, the geophysical and borehole data suggest that the Permian basalts extend over an area of ca. 250,000 $km^2$ in the Tarim Basin (Li et al. 2011). In addition, drill-hole data indicate that the basalts range from several metres to several hundreds of metres thick, with an estimated average thickness of ~300 m, suggesting a volume of more than 75,000 $km^3$ (Yu et al. 2011). According to the latest zircon U–Pb age results, the basalts in the Tarim Basin formed between 285 and 290 Ma (Tian et al. 2010; Yu et al. 2011). Furthermore, the Tabei uplift, the northern depression and the western region of the basin developed acid rocks, such as rhyolite and syenite. The area of rhyolite is approximately $0.46 \times 10^5$ $km^2$ (Pan et al. 2014), smaller than that of the basalt in the Tarim Basin. Based on the $Ar^{40}/Ar^{39}$ and SHRIMP test data, the acid rocks formed mainly between 274 and 284 Ma. Only in some northern parts of the basin do both basalt and rhyolite exist (Yang et al. 2006; Huang et al. 2012).

The SN 3-D seismic survey is located in the central part of the Tarim Basin and the eastern part of the Tazhong uplift (Fig. 1c). It is adjacent to the Manjiaer depression in the north and the Tangguzibasi depression in the south. The Permian System in the Tarim Basin consists of the Nanzha Formation, the Kupkuciman Formation, the Kaipeleicike Formation and the Shajingzi Formation, from bottom to top (Xinjiang Bureau of Geology and Mineral Resources, 1993). In addition, the Kupkuciman Formation primarily comprises a cycle from basic to acid volcanic rocks or from basic volcanic rocks to terrestrial clastic rocks (Pu et al. 2011). Based on drilling data, the lowermost Permian Nanzha formation is approximately 200 m thick. This formation mainly consists of grey mudstone and clastic rocks (Fig. 1d). The Kupukuziman Formation within the survey is approximately 100 m thick and contains one basalt layer in the lower part. This basalt layer differentiates the Kupukuziman Formation and the Nanzha Formation. Furthermore, alternating reddish mudstone and siltstone developed beyond the flood basalt (Fig. 1d). The Kupukuziman Formation is characterized by a natural positive-gamma cycle. The Kaipeleicike Formation within the survey area is also approximately 200 m thick and consists of mudstone and glutenite, with thick mudstone on the top part (Fig. 1d). The upper Shajingzi Formation has been eroded. The high-velocity volcanic rocks usually alternate vertically with the low-velocity terrestrial clastic rocks. Additionally, volcanic rocks display a very high-amplitude reflection on seismic sections and are therefore easily recognized and traced to determine their

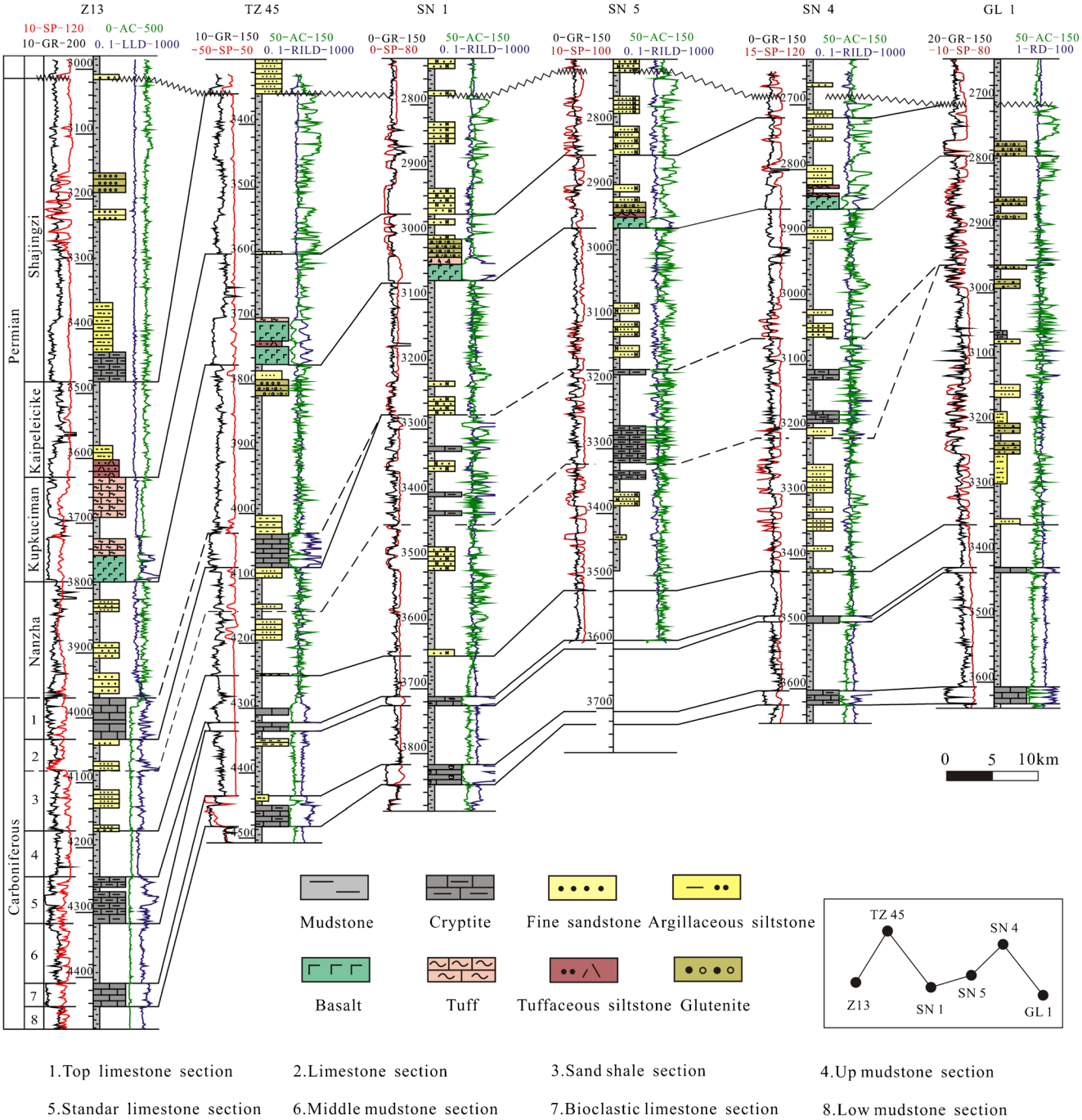


**Fig. 4** The Carboniferous-Permian stratigraphic cross-sections of wells Z13-TZ45-SN1-SN5–SN4-GL1 from the centre to the east of the basin; see Fig. 1c for the well locations

distribution based on integrated interpretation of 3-D seismic and well data (Pu et al. 2012).

## Database

The data used in this study consist of a poststack 3D seismic volume and wireline logs. The 3-D seismic survey covers an area of approximately 1195 km$^2$. There are 2700 lines and 2200 traces in this 3-D seismic volume with 25 and 25 m bin spacing, and the sampling interval is 2 ms. The dominant frequency is approximately 35 Hz. The P-wave velocity of volcanic rock is approximately 5800 m/s and of the overlying and underlying clasticstone are approximately 3500 m/s. The horizon of Permian volcanic rock ($T_5^1$) was picked for attribute extraction. The

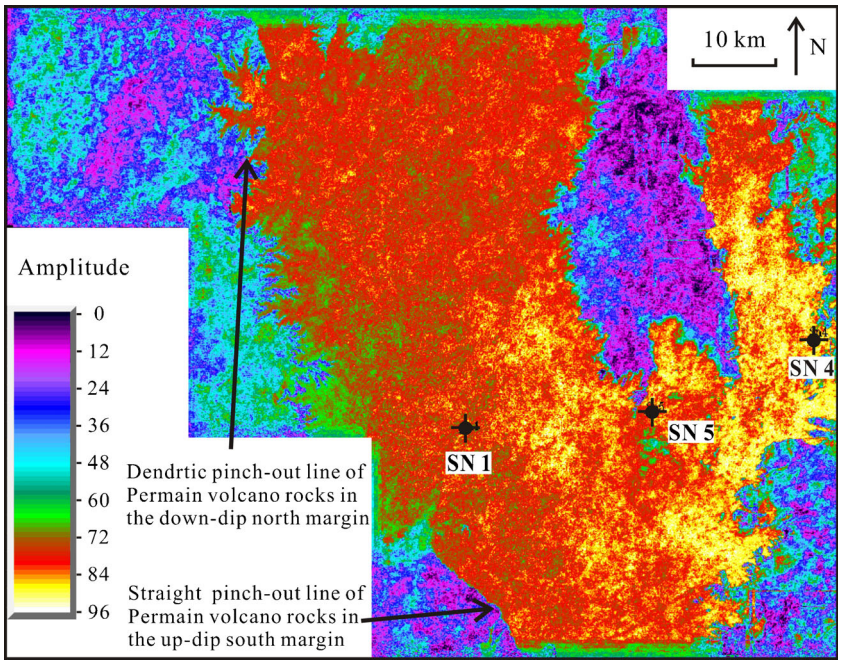


**Fig. 5** The maximum peak amplitude map of the volcanic rock horizon ($T_5^1 \pm 15$ ms) in the SN 3-D survey. The volcanic rocks show a distribution with two branches from south to north, and the high amplitude means thick volcanic rocks. See Fig. 1c for the location of the survey

$T_5^1$ horizon is shown as a continuous peak in entire seismic survey.

Since 2013, exploration wells SN1, SN4 and SN5 have been drilled within the survey area, and exploration wells SN2, SN3, GL1 and GL2 have been drilled near the survey area. The wells TZ45, Z13 and AD1 are distributed in the Tazhong area. Various combinations of natural gamma-ray, resistivity, density and acoustic logs are available for these wells. The Permian volcanic rocks and some Ordovician carbonate hydrothermal reservoirs were drilled in wells SN1, SN4 and SN5. Records of the gas production from the well SN4 indicate that study area produced commercial gas from the Ordovician carbonate reservoirs. No volcanic rocks were drilled in wells SN2 and SN3 adjacent to the survey area.

## Study of the Permian volcanic rocks

### Identification of the volcanic rocks lithology

Each type of volcanic rock exhibits a distinctive log response characteristic. The Permian volcanic rocks encountered in wells SN1, SN4 and SN5 within the SN survey are identified according to the well logging curves and ditch cutting data because cores are lacking. The volcanic rock type in the area is simple and mainly comprises flood basalt and tuffite generated from Permian magmatic activity. The basic basaltic magma effusived from the craters and formed the flood basalt. The great distribution extent of flood basalt is because of the lava's fluidity. The tuffites which are thin-bed interbed with different lava flow are located beyond the flood basalt. The nature gamma values of tuffites within the study survey are between 50~60 API. According to Zhang et al. (2014), the GR value of basic flow deposition tuffite is always between 40.84 and 64.48 API and of the fallout is always between 68.43 and 112.4 API. Moreover, the tuffite within study survey distributed in a narrow scope and near the volcanic craters, so they should belong to basaltic flow deposition. At the early period of flood basalt activity, the basaltic magma met the water-bearing layer underground when they upwelled and then intensive interaction occurred. This phenomenon has a certain relationship with the formation of the tuffite within study survey (Peate et al. 2003; Peate et al. 2005). No intrusive rocks are found in this area. The depth of flood basalt in well SN4 is 2841–2861 m, and its thickness is approximately 20 m. It is characterized by straight and low natural gamma (smaller than 50 API), a low acoustic time (50–70 μs/ft) and high resistivity (2–1000 Ωm) (Fig. 2). The flood basalt data from wells SN1, SN5 and SN4 show wide variations in their acoustic time, density, natural gamma and resistivity logs (Fig. 2). The resistivity and density are low (2 Ωm and 2.4 g/cm$^3$) at the flow top, gradually increasing to a maximum (1000 Ωm and 2.7 g/cm$_3$) in the flow core and then decreasing sharply at the flow base. In contrast, the natural gamma and acoustic times are high (47 API and 75 μs/ft) at the flow top, gradually decreasing to a minimum (33 API and 55 μs/ft) in the flow core and then increasing sharply at the flow base. This cyclical pattern in the wireline log data is often observed in flood basalt facies (Planke 1994; Bücker et al.

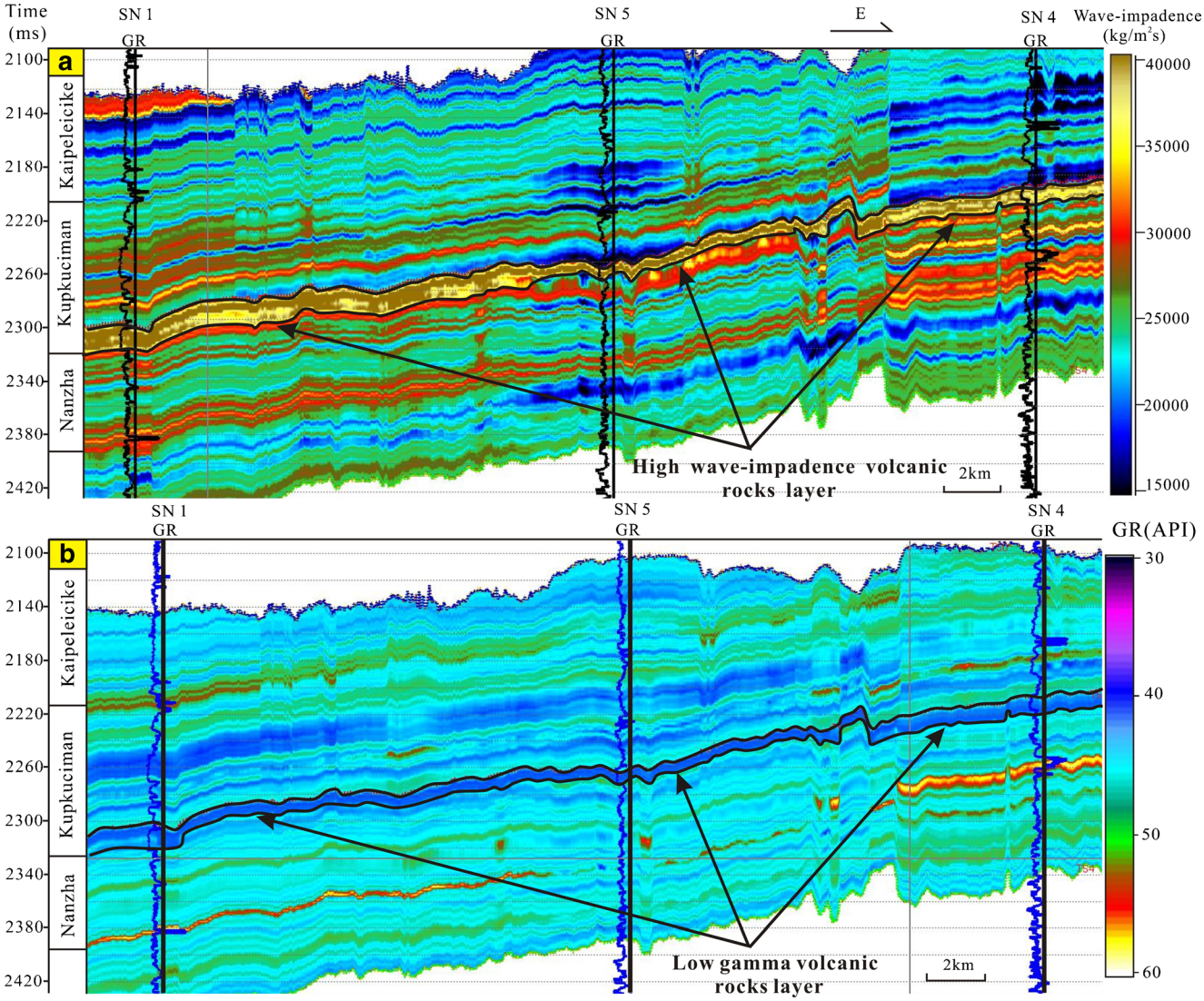


**Fig. 6** The well-tied wave impedance (**a**) and natural gamma ray (**b**) inversion profiles of wells SN1, SN5, and SN4; see Fig. 1c for the location of wells. The volcanic rocks are thicker in well SN1, thinner in well SN4 and thinnest in well SN5

1998) and is caused by the vertical variations in vesicularity and fracturing that characterize flow lobes of flood basalt (Nelson et al. 2009). On the top part, many vesicles and fractures reduce the sonic velocity and density. In addition, the top often shows a greater degree of alteration than other parts, resulting in a high gamma ray value. Because the flow core has low degrees of fracturing and vesicularity, the velocity and density are high. The Permian flood basalts in the three wells have natural gamma log values of approximately 37 API, but their average acoustic time values increase from west to east: well SN1, 50 μs/m; well SN5, 55 μs/m; and well SN4, 70 μs/m. In addition, the resistivity decreases to a certain extent. This phenomenon probably indicates that the eastern parts suffered severe alteration and secondary mineralization.

The cutting logging indicates that tuffite developed in wells SN4 and SN5 in the study area. These tuffites are similar to the core tuff from the adjacent area on the crossplot of volcanic logging (Fig. 3). The tuffites are characterized by high acoustic time (95 μs/ft) and low natural gamma values (45 API). However, it is very difficult to determine the source and components of the tuffites using only ditch cutting information. In addition, because some terrigenous materials mixed into the tuffite during the diagenetic process, the tuffite and terrigenous clastic rocks usually have similar or approximately identical log values. Therefore, because of the lack of core data, cuttings and logs are used to infer that the basalt is dominant in the area, with the occasional appearance of very thin tuffite.

## Volcanic stage and horizon

The Shunnan area Permian volcanic rocks are all categorized as effusive rocks. The magma upwelled along the volcanic feeders and condensed to rocks after erupting to form the craters. Thus,

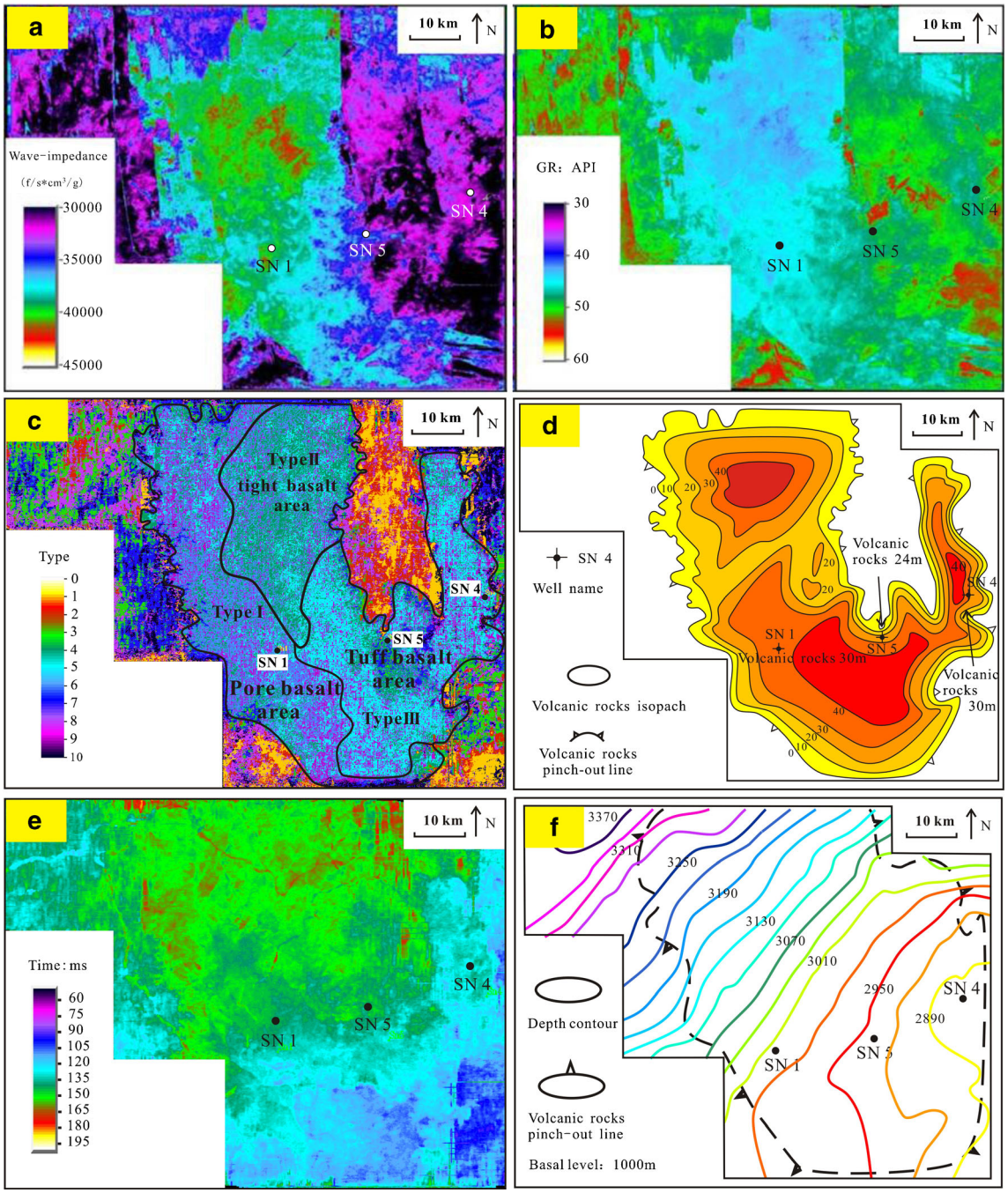


**Fig. 7** **a** The average inversion impedance map at the $T_5^1$horizon of volcanic rocks. **b** The average inversion gamma map at the $T_5^1$ horizon of volcanic rocks. **c** The waveform classification map of the reflection of volcanic rocks in the time window $T_5^1 \pm 15$ ms. **d** The thickness map of the volcanic rocks. **e** The time thickness map of the Lower Permian reflection from horizon $T_5^1$ to $T_5^4$. **f** The depth contour map of the top volcanic rocks

the areas where volcanic rocks are distributed have developed volcanic feeders, and the underlying stratigraphy experienced hydrothermal activity. Such hydrothermal activity has a vital influence on the formation of Ordovician dolomite hydrothermal reservoirs. Therefore, the location of the volcanic rocks and the lacuna type of the volcanic rocks (lack of deposition or erosion) both warrant further study.

Previous research studies have shown that volcanic rocks are mostly developed in the Permian Kupkuciman Formation and the Kaipeleicike Formation in the Tarim Basin (Pu et al. 2011). Based on the integrated interpretation of wireline logs, cuttings and seismic data, the wells in the SN survey contain Permian Kupkuciman volcanic rocks that were deposited in a restricted area. The Kaipeleicike Formation in the 3-D survey

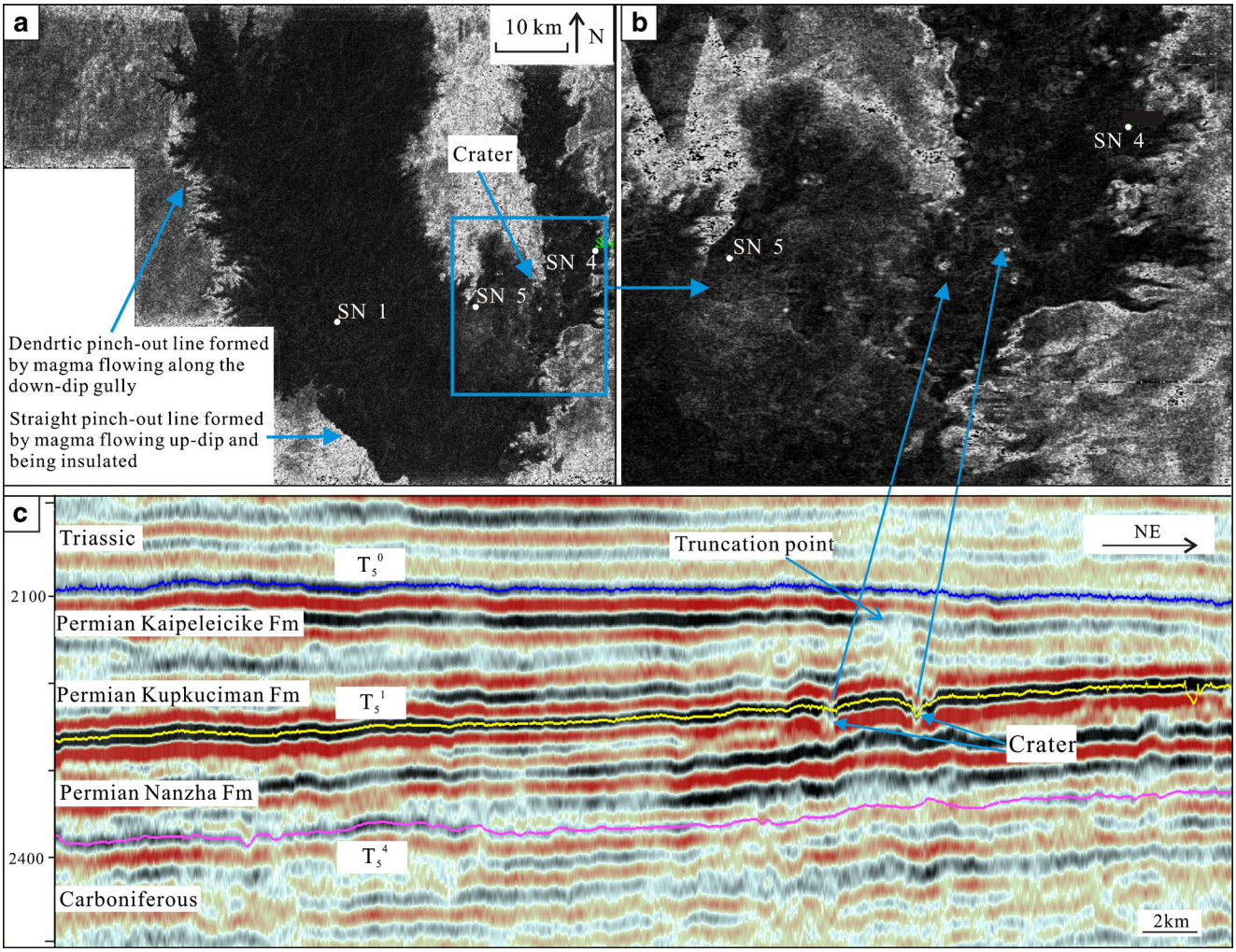


**Fig. 8** **a** A coherent slice map along the $T_5^1$ horizon within the SN 3-D survey, where the *small white dots in the blue rectangle* are craters. See Fig. 1c for the location of survey. **b** Enlarged view of the *blue rectangle*, with the volcanic craters shown as *small white dots*. **c** The seismic section across the crater, showing the bending and decrease in the amplitude at the craters of the $T_5^1$ volcanic reflection event

was subjected to incomplete denudation, and no volcanic rocks were drilled (Fig. 4).

The lowermost Permian Nanzha Formation is lithologically stable within the whole basin and is primarily composed of dark-coloured marls and light-coloured chalks with locally interbedded silt to fine sandstone (Guo et al. 2011). The Nanzha Formation is easily identified by the underlying disconformity contact with the Carboniferous Kalashayi Formation limestone and is overlain by Kupkuciman Formation volcanic rocks (Fig. 4). Based on the existence of the Nanzha Formation and volcanic rocks, the cycle from low natural gamma volcanic rock to high natural gamma terrigenous silicic clastic rock situated above the Nanzha Formation in wells SN1, SN5 and SN4 should belong to the Kupkuciman Formation. No volcanic rocks were drilled in the Kaipeleicike Formation, and the uppermost Permian Shajingzi Formation was eroded out completely from wells SN1, SN5 and SN4 (Fig. 4). The above stratigraphic correlation confirms that no volcanic rock of the Kaipeleicike Formation occurs in the SN1 3-D survey; thus, the volcanic rock observed here should belong to the Kupkuciman Formation. No volcanic rock in the Permian Kupkuciman Formation is contained in the wells outside of the SN1 3-D survey (e.g. GL1, GL2, SN2 and SN3); however, equivalent strata exist, with lithologies changed to sandstone or sandy conglomerate. Therefore, the pinch-out of volcanic rocks in the SN1 3-D survey likely resulted from the lack of deposition. Compared with the wells in the Tazhong and Tahe regions, the Carboniferous System in wells SN1 and SN4 contains the Standard Limestone section and the Bioclastic Limestone section; similar findings were noted in well TZ45 (Fig. 4). After the Permian Period, intense uplift occurred in the Tadong and Bachu regions, and the remaining Permian System thickness decreases eastward. The Permian Kaipeleicike Formation around the SN1 3-D survey is more likely to be eroded to varying degrees. However, it is free of volcanic rock.

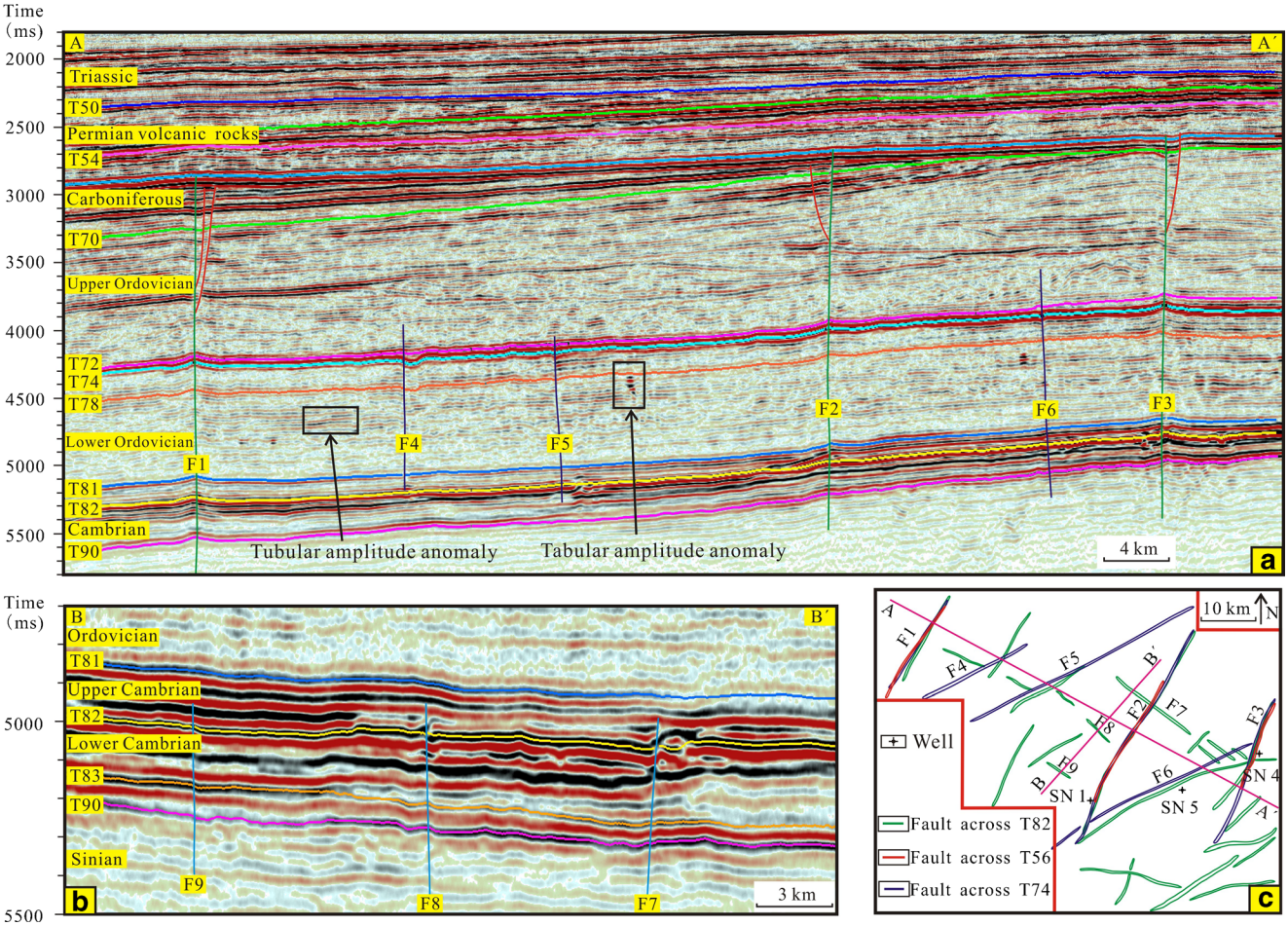


**Fig. 9** The seismic responses of three sets of faults in the SN3-D survey: NNE, NEE and NWW trending. **a** The profile of NWW fault ( *A*–*A*'). **b** The profile of NEE fault ( *B*–*B*'). **c** The map of the three sets of faults in the SN3-D survey

## Distribution of volcanic rock and changes in lithofacies

The volcanic rock typically shows high-amplitude reflections on the seismic sections (Pu et al. 2012). The distribution range and thickness change of volcanic rocks can be determined by the integrated interpretation of seismic attributes and inversion. The high-amplitude reflection at the volcanic horizon ($T_5^1$) is caused by the large wave impedance contrast between

**Table 1** The elements of three groups of differently trending faults in the SN 3-D survey

| Fault name | Fault's location in 3-D survey | Fault's plane orientation | The horizon be cut | | Active period | Fault's property | Spreading length (m) | Attitude of the fault zone |
|---|---|---|---|---|---|---|---|---|
| | | | Latest | Oldest | | | | |
| F1 | West part | NNE | $T_5^6$ | $T_9^0$ | $O_3$ started, P revived | $O_3$-$S_1$k compression-shear; $S_2$t and P transtensional | 20 | $O_3$ Upwarp but $T_6^0$-$T_5^1$ Pull down |
| F2 | Center | | | | | | 42 | |
| F3 | East part | | | | | | 20 | |
| F4 | Northwest | NEE | $T_7^2$ | $T_9^0$ | $\in_2$-$O_3$l | Transtensional | 14 | Pull down |
| F5 | Center to North | | | | | | 38 | Pull down |
| F6 | Center to south | | | | | | 40 | Pull down |
| F7 | Center | NWW | $T_8^1$ | $T_9^0$ | $\in_2$ | Transtensional | 14 | Pull down |
| F8 | Center | | | | | | 5.4 | Not obvious |
| F9 | Center | | | | | | 3.7 | Not obvious |

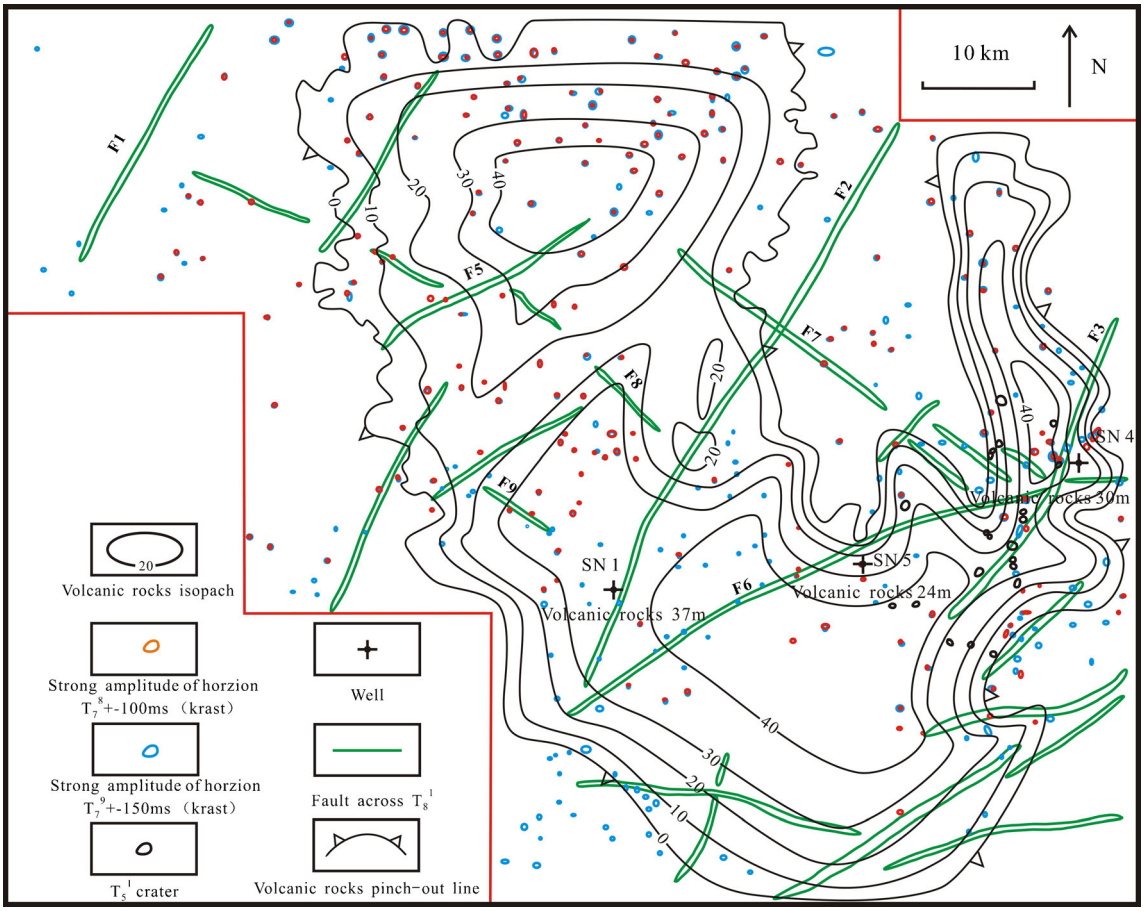


**Fig. 10** The relationships among the Ordovician high-amplitude anomalies and faults, the volcanic craters and the thicknesses of volcanic rocks in the 3-D survey. See Fig.1.c for the location of survey. The craters developed on both sides of the NNE faults near well SN4, and their positions are related to the intersections of the dense early NEE and NWW faults and the late NNE faults

volcanic rock with high wave impedance and sandy mudstone with low wave impedance. Therefore, high-amplitude areas on the amplitude map typically correspond to the distribution of volcanic rocks. The maximum wave crest amplitude attribute (Fig. 5) extracted along the $T_5^1$ ± 15-ms time window indicates that the volcanic rocks in the 3-D survey show a distribution with two branches from south to north, with the larger branch in the NNW direction (70 km long and 30 km wide) and the smaller branch in the NNE direction (20 km long and 2–5 km wide). The volcanic rock margin shows a branching zigzag pinch-out line in the downdip direction to the north and northwest but a straight pinch-out line in the higher south, suggesting a steep southern updip ancient landform with completely obstructed magma and a gentle smooth northern downdip slope on which lava flowed forward until terminated.

Wells SN2, SN3 and GL1 are located outside the depositional range of the volcanic rocks, and thus, the absence of volcanic rock in these wells is attributable to a lack of deposition rather than erosion. The spatial distribution of volcanic rock and lateral changes in lithology and thickness can be interpreted from well-constrained seismic inversion data on wave impedance and natural gamma values. Indeed, the wave impedance and natural gamma inversion profiles show that volcanic rocks are thicker in well SN1, thinner in well SN4 and thinnest in well SN5 (Fig. 6). The wave impedance within the range of volcanic rocks is uneven in distribution. Some minor uneven variations in the wave impedance of basalt between wells SN1 and SN5 suggest a change in the lithology or pore gas content. A decreasing trend of wave impedance exists from west to east, whereas the natural gamma values remain nearly unchanged.

The wave impedance values of volcanic rocks near wells SN4 and SN5 are much lower than those near well SN1 (Fig. 7a). In contrast, the natural gamma values of volcanic rocks near wells SN4 and SN5 are slightly higher than those near well SN1 (Fig. 7b). The higher wave impedance and lower gamma ray values in the west near well SN1 indicate pure basalt rock. The high gamma values and low wave impedance in the east near wells SN4 and SN5 indicate that the volcanic rocks contain more tuff or pores. The processed waveform classification of the volcanic horizon ($T_5^1$ ± 15 ms) is used to divide the waveforms of volcanic rocks into ten types in terms of lava thickness, natural gamma

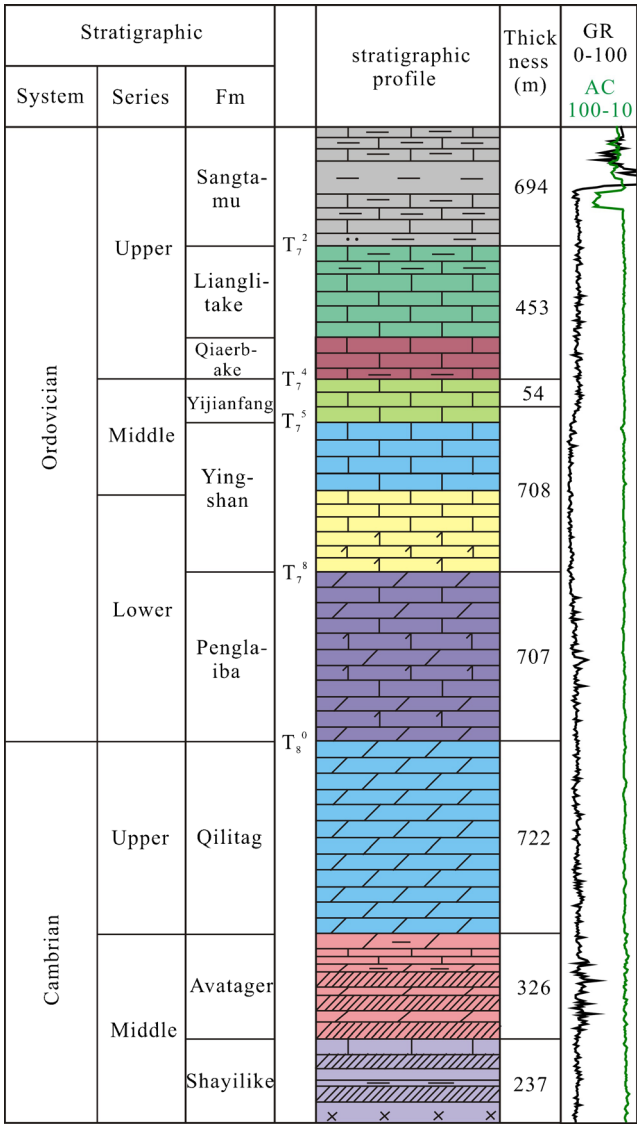


**Fig. 11** The Cambrian-to-Ordovician stratigraphic column of Shunnan area in Tarim Basin (modified by Zhao, 2012)

values, wave impedance and density. Different colours indicate different facies. Combining the inversion results (Figs. 7a, b) and the waveform classification reveals three facies zones in the Permian volcanic rock in the SN 3-D survey. These three seismic facies zones are a compact basalt facies zone with maximum wave impedance (40,000–46,000 f/s*cm$^3$/g) and minimum natural gamma (38–43 API), a pore-bearing basalt facies zone with medium wave impedance (37,000–41,000 f/s*cm$^3$/g) and natural gamma (45–50 API) and a tuffaceous basalt facies zone with lower wave impedance (30,000–33,000 f/s*cm$^3$/g) and higher natural gamma (50–55 API) (Fig. 7c). The flood basalt thickness of the compact basalt facies zone is the greatest (exceeding 40 m) because of its low topography. Thus, the natural gamma value here is low, which is in good agreement with the inversion results. Wells SN4 and SN5 are located in the tuffaceous basalt facies zone, and both developed thin sedimentary tuff beyond the flood basalt layer (Fig. 2), which resulted in their high natural gamma values. The pore-bearing basalt facies zone is located at the margin of the volcanic rocks and has experienced alteration, which has been shown to increase the gamma values in basaltic rocks (Planke et al. 1999 ).

The volcanic rock thickness map is drawn according to the relationship among the tuning amplitude, the thickness of volcanic rock and the wave impedance inversion result (Fig. 7d). It clearly shows the two largest thickness centres with maximum thicknesses of approximately 40 m. The thicker area in the northwest corresponds to the high inversion wave impedance of volcanic rocks. Based on previous research on volcanic rocks in the Tahe field (Pu et al. 2012) and the south rifts of Songliao Basin (Wang et al. 2003), the flood basalt is thicker in the ancient lower topography because of lava downdip flow and accumulation. Therefore, the considerable thickness of the flood basalts in the northwestern SN 3-D survey was caused by the low palaeogeomorphology in this direction.

The $T_5^4$-$T_5^1$ stratigraphic thickness map approximates the depositional thickness of the lower Permian Nanzha Formation to the Kupkuciman Formation. Because the Kupkuciman Formation was not subjected to later denudation, the thickness map reflects the overall ancient structural or topographic background when the volcanic rocks were being deposited. It shows a north-dipping ancient structure (Fig. 7e) and lava flowing from south to north after eruption. This ancient structural feature is consistent with the current structure of the top volcanic rocks (Fig. 7f).

## Crater characteristics and distribution

Previous observations of volcanic craters have always been based on field work and laboratory studies, and analysing the geochemistry and petrography has played an important role. However, with the improvement of 3-D seismic data, seismic profiles can reveal the location, external form and internal structural characteristics of many craters (Joppen and White, 1990; Hansen, 2006; Magee et al. 2013; Hansen and Cartwright 2006). In addition, the seismic characteristics can also provide valuable evidence for studying the magma's intrusion and eruption mechanisms, the factors that control magmatism and several other important issues.

The volcanic craters in the Tazhong area have arch reflections, weak amplitude coherence anomalies, increased thickness and are rich in volcanic explosion facies (Pu et al. 2012). These craters have a direct relationship with magmatism. The basaltic magma upwelled along the volcanic feeders and erupted from these craters. The feeders cannot be seen on the seismic profile because their diameters are always less than 100 m in the Tazhong area. The craters consistently developed around the intersections of multi-set faults. The crater

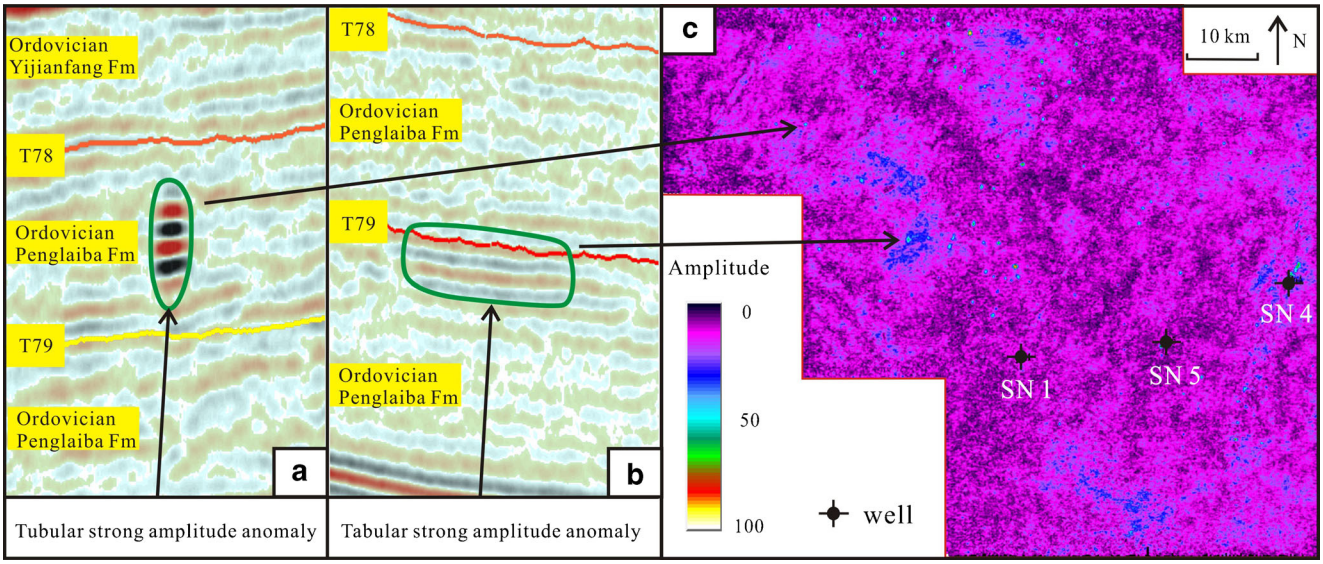


**Fig. 12** **a** The profile shape of the tubular high-amplitude anomalies. **b** The profile shape of the tabular high-amplitude anomalies. **c** The planar graph of the $T_7^8$ + 80 ms average reflection intensity amplitude. See Fig. 1c for the location of survey

diameters are typically 200–500 m and are sometimes unclear in the seismic profiles.

The craters in the 3-D area are clearly shown in both volcanic horizon slices of the coherence cube (Fig. 8a, b) and the seismic profile (Fig. 8c). The craters on the horizon ($T_5^1$–5 ms + 20 ms) slice of the coherence cube of the research area are characterized by circular low coherence, with the crater diameters ranging from 100 to 1000 m (mainly 200 to 500 m). The craters in the south to the midpoint between wells SN4 and SN5 (Fig. 8b) and around the NNE fault zone of well SN4 are located in a rectangular area (5 km wide and 20 km long along the northeast direction); the distance between craters ranges from 1 to 10 km (typically 2 to 4 km) for approximately 18 craters, among which the 9 larger craters are remarkable. The craters are similar to the modern basalt craters seen in Wudalianchi, Australia (Blaikie et al. 2014) and Japan (Kenji et al. 2014) in terms of their scale.

The $T_5^1$ event of the crater position on the seismic profile shows weak amplitude and fall-down and subsequent fill-up at the location of the fall. The overlying horizon $T_5^4$ and underlying horizon $T_5^0$ do not change in their attitude. The fall-down of the volcanic rock surface is attributable to the condensation and contraction of magma at the crater and local subsidence. The fall-down event indicates the collapse of the volcanic rocks, with the overlying deposits subsequently filling and levelling the collapse. The attitudes of the formations overlying and underlying the crater remain horizontal. These features typically form craters with basic magma, whereas the acidic magma craters observed in the Tahe field and the Songliao basin readily take on mound-shaped appearances

**Table 2** Ordovician Yijianfang Formation andCambrian system high-amplitude anomaly-type statistics in the SN 3-D area

| Stratigraphic | Horizon | High amplitude anomaly types | | | |
|---|---|---|---|---|---|
| | | Tubular anomaly | | Tabular anomaly | |
| | | Quantity | Frequency (%) | Quantity | Frequency (%) |
| $O_2yj$ | $T_7^4 \sim T_7^5$ | 5 | 0.7 | | |
| $O_{1\sim2}y$ | $T_7^5 \sim T_7^5$ + 80 ms | 10 | 1.4 | 10 | 10.4 |
| $O_{1\sim2}y$ | $T_7^8 \sim T_7^8$-80 ms | 15 | 2.1 | 9 | 9.4 |
| $O_1p$ | $T_7^8 \sim T_7^8$ + 80 ms | 115 | 16.2 | 5 | 5.2 |
| $O_1p$ | $T_7^8$ + 80 ms ~ $T_7^8$ + 160 ms | 220 | 30.9 | 3 | 3.1 |
| $O_1p$ | $T_7^9 \sim T_7^9$-80 ms | 83 | 11.7 | 15 | 15.6 |
| $O_1p$ | $T_7^9 \sim T_7^9$ + 80 ms | 50 | 7.1 | 4 | 4.2 |
| $O_1p$ | $T_7^9$ + 80 ms ~ $T_7^9$ + 160 ms | 136 | 19.1 | 12 | 12.5 |
| $O_1p$ | $T_8^0 \sim T_8^0$-80 ms | 40 | 5.6 | 15 | 15.6 |
| $\in 3ql$ | $T_8^0 \sim T_8^0$ + 80 ms | 24 | 3.4 | 11 | 11.5 |
| $\in 3ql$ | $T_8^0$ + 80 ms ~ $T_8^0$ + 160 ms | 13 | 1.8 | 12 | 12.5 |

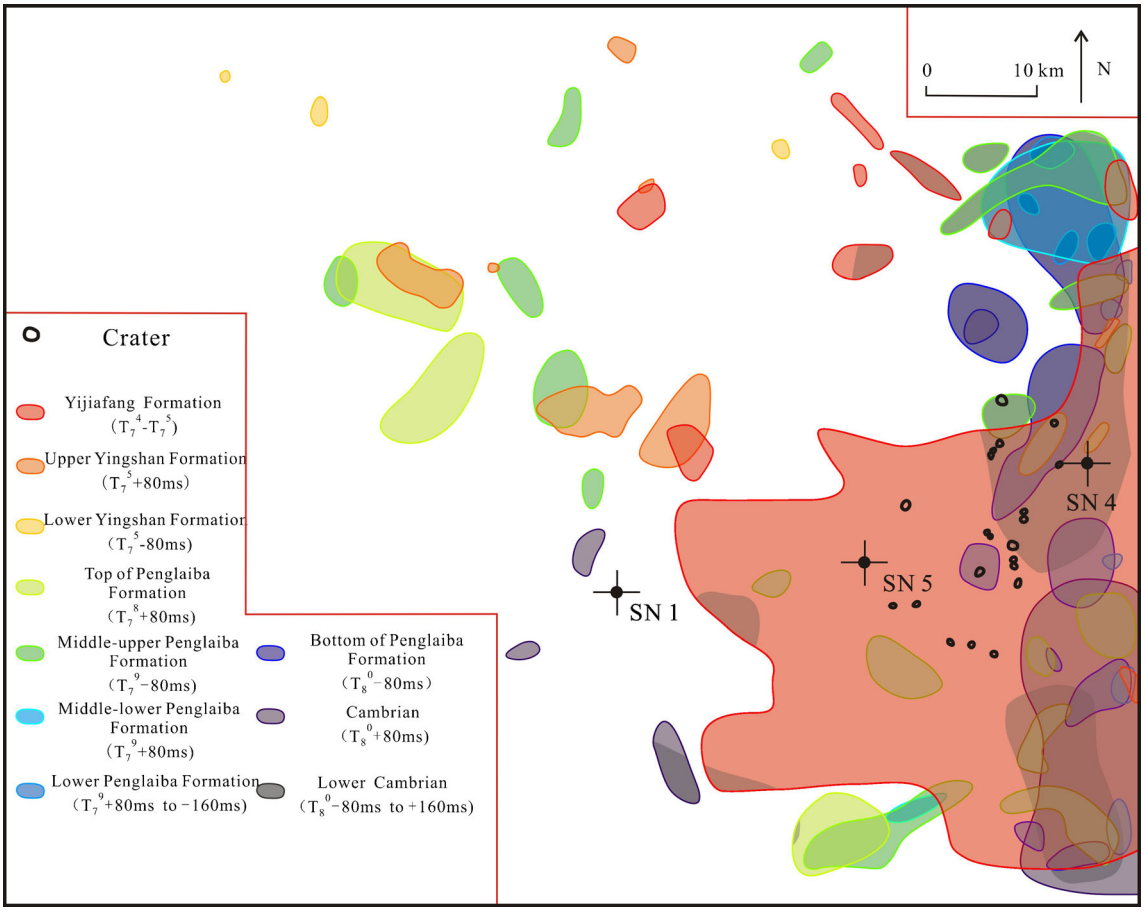


**Fig. 13** The relationship between the high-amplitude anomalies of the Ordovician carbonate rocks and the locations of volcanic craters, showing similar development and distribution patterns. See Fig. 1c for the location of survey

because of their high magma viscosity, weak mobility and palaeo-topography.

## Relationship between volcanic rock and faults

Faults are likely the channels for volcano formation and magmatism (England et al. 1987; Wu et al. 2012b). The Tarim Basin experienced multi-stage tectonic movements and includes hundreds of faults with different locations, stages, properties and dimensions (Coleman et al. 1989; Allen et al. 1999; Ren et al. 2011). The faults in the Tarim Basin are mainly NW, NE and E-W trending (Yan et al. 2014). There are three sets of vertical faults within the 3-D survey: NNE, NEE and NWW. The NWW set of faults and NEE set of faults are shown in Figs. 9a, b, respectively. The dip angles of these strike-slip faults are close to vertical, and the displacements are small. The flower structure can be seen in profiles, and the faults are characterized by an en echelon distribution in a planar view (Fig. 9c). Detailed examination of the 3-D seismic profile reveals that the strata thicknesses at the vertical fault zone differ from those of the bilateral fault sides at the same period. Moreover, the horizons of the fault zone pull down as their thicknesses increase but pull up as their thicknesses decrease. The former are identified as synsedimentary tension-shear faults, and the latter are classified as synsedimentary compression-shear faults. Based on the insight into the fault properties and active phases presented above, we conclude that in the 3-D survey, the NEE and NWW faults are conjugate and syngenetic transtensional faults from the early Caledonian period. From the Middle Cambrian period, the NWW faults subsequently stopped their activity. After the standstill episode in the Late Cambrian period to the Early Ordovician period, however, the NEE faults initiated transtensional action in the initial depositional stage of the Middle Ordovician Lianglitage Formation and then became quiet at the end of deposition of this formation. NNE faults resumed their syngenetic and compressive actions from the Late Ordovician Sangtamu Formation to the Early Silurian Kepingtage Formation and then exhibited transtensional movement during the deposition of the Middle Silurian Tataaiertage Formation. During the Devonian-Carboniferous period, the NEE faults remained dormant, but in the Permian System, they were revived by the upward movement of magma. Briefly, the NNE faults are the latest, the NEE faults are earlier and NWW are the earliest (Table 1).

The planar relationship between the three sets of faults and the craters is shown in Fig. 10. The craters are primarily located near the intersections between the NWW fault F7 and the NNE fault F3. The volcanic rocks on both sides of the NNE fault F3 are the thickest (up to 40 m). The NWW fault F7 furcates into three small ones close to the craters from an individual fault in the centre of the study area far away from the craters, showing an apparent increase in the fault density or a decrease in the fault interval from 10 to 2–3 km near the craters. The older Caledonian faults were the passageways for magma flowing from the deep strata to the shallow strata, and the newer Hercynian faults allowed lava to erupt through the surface from underground. This spatial distribution of craters accounts for the joint contribution to the intensity and intersection of multiple set of faults instead of only the newer-stage Permian faults when the volcanoes were erupting.

## Relationship between volcanic rock and hydrothermal activity

The outcrop and volcanic dating analysis shows that four major times of magma activity and geological thermal events exist in the Tarim Basin—the Sinian-Cambrian period (774 ± 0.18 ~ 673.1 ± 55.4 Ma), the Ordovician period (460.2 ± 2.2 ~ 484.5 ± 2.2 Ma), the Permian period (26 ~ 282 Ma) and the Cretaceous period (100.9 ± 3.4 Ma)—of which the Permian magma activity is the most intense and the most extensive in distribution (Chen et al. 1997). The generation of hydrothermal fluid should be closely related to volcanic magma, and the magmatic fluid and hydrothermal fluid reworked by magma in adjacent strata dissolved the Ordovician carbonate rocks when migrating along the faults and fissures (Jin et al. 2006).

The Tarim Basin Cambrian-to-Ordovician strata form a marine sedimentary system that mainly comprises carbonate rocks. The Tazhong area developed the Middle Cambrian Shayilike Formation ($\in_2$S) and Avatager Formation ($\in_2$a), the Upper Cambrian Qiulitag Formation ($\in_3$ql), the Lower Ordovician Penglaiba Formation ($O_1$p), the Lower-Middle Ordovician Yingshan Formation ($O_{1\sim2}$y), the Middle Ordovician Yijianfang Formation ($O_2$yj) and the Upper Ordovician Qiacrbake Formation ($O_3$q), Lianglitake Formation ($O_3$l) and Sangtamu Formation ($O_3$S) (Fig. 11). Contacts between these formations are conformable or paraconformities (Zhang and Gao 1992). The Cambrian and Penglaiba Formations mainly comprise dolomite rocks and are interbedded with thin limestone and calcitic dolomite. The lower Yingshan Formation is primarily composed of calcitic dolomite, and the upper Yingshan Formation mainly consists of limestone. The dolomitic component exhibits an obvious decrease from bottom to top (Zhao et al. 2012). The Yingshan Formation developed large amounts of hydrothermal dolomite and thermally dissolved pores, which occurred along the faults and paraconformity planes. This set of hydrothermal dolomite reservoirs is one of the most significant gas reservoirs within the Tarim Basin.

There is no unconformity or disconformity between the Ordovician carbonate rocks and the overlying Qiaerbake Formation and Lianglitage Formation. No hiatus occurs within the Ordovician Penglaibaba Formation, Yingshan Formation and the Yijianfang Formation. Thus, the talpatate karst of the Ordovician carbonate rocks is not the main dissolution type. The burial dissolution and organic acid dissolution are related to hydrocarbon generation, and the entrances into the reservoir exhibit limited dimensions and strength. On the seismic sections, therefore, the many karst-related high-amplitude reflections (narrow vertical bead reflections) observed in the weak amplitude background of the thick Ordovician carbonate rocks did not originate from buried karst or talpatate karst. The Ordovician limestone reservoir that produced oil and gas and displays many dissolved vugs on the cores in the well SN4 should have formed principally via hydrothermal dissolution.

Hydrothermal fluid carries abundant volatile substances, such as organic acids, $CO_2$, $H_2S$ and $SO_2$. These substances entered into reservoirs along faults, fissures, bedding, unconformities and other pores, forming a large number of tubular and tabular caves or vugs through karst alteration of the surrounding limestone. These cave-related reservoirs show exceptionally strong vertical bead reflections or horizontal anomalies on their seismic sections (Fig. 12a, b). The tubular caves appear as dots on the plane and cover areas smaller than 0.3 $km^2$, whereas the tabular caves appear as flakes on the plane and cover areas exceeding 0.3 $km^2$ (Fig. 12c). The analysis shows that the tubular anomalies are distributed widely throughout the 3-D survey and that the high-amplitude tabular anomalies are primarily distributed in the eastern and southern parts of the survey. We also analysed the Reconnaissance Map Series (RMS) maps extracted from the Yijianfang Formation ($O_2$yj, $T_7^4$) to the bottom of the Cambrian system ($T_8^0$ + 160 ms) with an interval of 80 ms. The high-amplitude anomaly statistics (Table 2) show that the distribution of high-amplitude tubular anomalies is concentrated in the Penglaiba Formation (horizons $T_8^0$-$T_7^8$), accounting for 85 % of all tubular anomalies, whereas the tabular anomalies are mainly distributed in the lower Penglaiba Formation and the Cambrian system (under $T_7^9$), accounting for 71.9 % of all tabular anomalies. Why are the tubular caves more likely to develop in the Penglaiba Formation than in the Yingshan Formation and the Yijianfang Formation? One reason is that the carbonate rocks in the Early Ordovician Penglaiba Formation were more likely to be subjected to

hydrothermal processes than those in the later Yingshan Formation and Yijianfang Formation because the Penglaiba Formation experienced one more magma and hydrothermal fluid reworking event in the Early Ordovician period than the other, later deposited carbonate rocks of the Yingshan Formation and the Yijianfang Formation.

Although no correlation between the distribution range of the tubular high amplitude and the craters and faults was observed, the tabular karst caves and craters have similar development and distribution patterns: they are all concentrated in the dense old fault zone or the intersections between new and old faults (Fig. 13). The thickness of the high amplitude relevant to the karst is increased in the intersection between the new and old fault zones. Similar to the volcanic activity, the distribution of these flaky karst caves is also concentrated in the dense fault zone and the intersections between new and old faults. NEE and NWW old faults broke and dislocated rock at depth and reduced their strength, thereby allowing the magma and hydrothermal fluid to upwell and dissolve the surrounding carbonate rocks.

## Conclusions

1. Permian volcanic rock in the SN3-D survey is primarily composed of basalt and tuffite rocks, which constitute the lower Permian Kupkuciman Formation. Above this, the Kaipeleicike Formation consists of terrigenous clastic rock, and the Shajingzi Formation is denuded. The absence of volcanic rock near wells SN2 and GL1 is attributed to lack of deposition. The Permian volcanic magma in the survey erupted and flowed northwestward along a furcating low ravine under the ancient northwest dip topographic background, creating a northward branching lobe of volcanic rocks. The lobe shows a dendritic pinch-out line in the down-dip north boundary and a straight pinch-out line in the steep up-dip south boundary.
2. Three sets of faults developed in the 3-D survey, namely NNE, NEE and NWW trending, with craters developed on both sides of the NNE fault near well SN4. The crater positions are related to the intersections of the dense early (Caledonian period) NEE and NWW faults and the late (Hercynian period) NNE faults. The older Caledonian faults allowed magma to flow from deep to shallow strata, and the newer Hercynian faults provided a path for the Permian magma to erupt through the surface from the shallow strata.
3. The Ordovician limestone reservoir can be primarily attributed to hydrothermal dissolution in the 3-D survey. A large number of tubular and tabular high-amplitude anomalies are evident in the Ordovician carbonate rock reflection profiles. These anomalies resulted from the hydrothermal dissolution that occurred in the Penglaiba Formation and its surrounding carbonate rocks. The distribution of Ordovician tabular high-amplitude anomalies that are possibly related to the hydrothermal dissolution of carbonate rocks is similar to that of the Permian craters. Both of these structures were affected by the intensities and intersections of multiple sets of faults.

**Acknowledgments** Comments from two anonymous reviewers and editors of AJGS are gratefully acknowledged in improving this manuscript. I wish to thank Professor Renhai Pu's kind help with this research. We would like to acknowledge Sinopec Northwest oil field branch for helpful discussions and access to data. This study was financially supported by the major program of the National Natural Science Foundation of China titled "characteristics and classification of the non-conventional oil and gas reservoirs in China and establishment of typical geological models of these reservoirs" (grant number: 41390451) and the enterprise project of Sinopec Northwest oil field branch.

## References

Allen MB, Vincent SJ, Wheeler PJ (1999) Late Cenozoic tectonics of the Kepingtage thrust zone: interpretation of the Tienshan and Tarim Basin, Northwest China. Tectonics 18(4):639–654

Arndt NT, Chauvel C, Fedorenko V, Czamanske G (1998) Two mantle sources, two plumbing systems: tholeiitic and alkaline magmatism of the Maymecha River basin, Siberianflood volcanic province. Contrib Mineral Petrol 133:297–313

Blaikie, Ailleres L, Betts PG, Cas RAF (2014) A geophysical comparison of the diatremes of simple and complex maar volcanoes, newer Volcanics Province, South-Eastern Australia. J Volcanol Geotherm Res 276:64–81

Bücker CJ, Delius H, Wohlenberg J, Leg 163 Shipboard Scientific Party (1998) Physical signature of basaltic volcanics drilled on the Northeast Atlantic volcanic rifted margins. In: Harvey PK, Lovell MA (eds) Core–log integration, vol 136. Geological Society, London Special Publications, pp. 363–374

Campbell IH, Czamanske GK, Fedorenko VA, Hill RI, Stepanov V (1992) Synchronism of the Siberian traps and the Permian-Triassic boundary. Science 258:1760–1763

Chen HL, Yang HF, Dong CW, Zhu GQ, Jia CZ, Wei GQ, Wang ZG (1997) The study of geology thermal event of Tarim Basin. Chin Sci Bull 42(10):1096–1098 in Chinese with English abstract

Chen HL, Yang HF, Wang QH, Luo JC, Jia CZ, Wei GQ, Li ZL, He GY, Hu AP (2006) Sedimentary response to the Early-Mid Permian basaltic magmatism in the Tarim plate. Geol China 33(3):545–552 in Chinese with English abstract

Chen MM, Tian W, Zhang ZL, Pan WQ, Song Y (2010) Geochronology of the Permian basic intermediate acidic suite from Tarim, Northwest China and its geological implications. Acta Petrol Sin 26(2):559–572 in Chinese with English abstract

Chung SL, Jahn BM (1995) Plume–lithosphere interaction in generation of the Emeishan flood basalts at the Permian-Triassic boundary. Geology 23:889–892

Coleman RG (1989) Continental growth of Northwest China. Tectonics 8(3):621–635

Derek W (2003) Mantle plumes: their identification through time. Geological Society of America special paper 352. Econ Geol 98: 669–670

England W, MacKenzie AS, Mann DM, Quigley TM (1987) The movement and entrapment of petroleum fluids in the subsurface. *Journal of Geological*. Society 144:327–347

Ernst RE, Buchan KL (2003) Recognizing mantle plumes in the geological record. *Annual Reviews of Earth and Planetary*. Science 31: 469–523

Guo Q, Pu RH, Xu J, Tian YY, Fan TT (2011) Strata correlation and sedimentary facies analysis of Nanzha formation, Tarim Basin. J Northwest Univ (Nat Sci Ed) 41(3):491–496 in Chinese with English abstract

Hansen DM (2006) The morphology of intrusion-related vent structures and their implications for constraining the timing of intrusive events along the NE Atlantic margin. J Geol Soc 163(5):789–800

Hansen DM, Cartwright J (2006) Saucer-shaped sill with lobate morphology revealed by 3D seismic data: implications for resolving a shallow-level sill emplacement mechanism. J Geol Soc 163(3): 509–523

Huang H, Zhang ZC, Kusky T, Santosh M, Zhang S, Zhang DY, Liu JL, Zhao ZD (2012) Continental vertical growth in the transitional zone between south Tianshan and Tarim, western Xinjiang, NW China: insight from the Permian Halajun A1-type granitic magmatism. Lithos 155:49–66

Jin ZJ, Zhu DY, Hu WX, Zhang XF, Wang Y, Yan XB (2006) Geological and geochemical signatures of hydrothermal activity and their influence on carbonate reservoir beds in the Tarim Basin. Acta Geol Sin 80(2):245–253 in Chinese with English abstract

Joppen M, White RS (1990) The structure and subsidence of Rockall trough from two-ship seismic experiments. J Geophys Res 19: 19821–19837

Kenji N, Rumi S, Hideki W, Tatsuya T, Hirochika S, Toshiya M, Urumu T, Pedro AH, Yusuke S, Ryoya I, Kohei O, Masato K, Toshiaki M, Naoyuki F (2014) Leakage of magmatic–hydrothermal volatiles from a crater bottom formed by a submarine eruption in 1989 at Teishi knoll, Japan. J Volcanol Geotherm Res 270:90–98

Li ZL, Chen HL, Song B, Li YQ, Yang SF, Yu X (2011) Temporal evolution of the Permian large igneous province in Tarim Basin in northwestern China. J Asian Earth Sci 42:917–927

Li YQ, Li ZL, Yu X, Yang SF, Chen HL, Tang ZL, Song B, Zou SY (2014) Origin of the Early Permian zircons in Keping basalts and magma evolution of the Tarim large Igneous Province (northwestern China. Lithos 204:47–58

Long XP, Yuan C, Sun M, Kröner A, Zhao GC, Wilde S, Hu AQ (2011) Reworking of the Tarim Craton by underplating of mantle plume-derived magmas: evidence from Neoproterozoic granitoids in the Kuluketage area, NW China. Precambrian Res 187(1-2):1–14

Luo JL, Zhai XX, Pu RH, He FQ, Zhao HT, Yu RL, Zhou JJ (2006) Horizon, petrology and lithofacies of the volcanic rocks in the Tahe oil field, Northern Tarim Basin. Chin J Geol 41(3):378–391 in Chinese

Magee C, Hunt-Stewart E, Jackson CAL (2013) Volcano growth mechanisms and the role of sub-volcanic intrusions: insights from 2D seismic reflection data. Earth Planet Sci Lett 373: 41–53

Mahoney J, Coffin M (1997) Large igneous provinces: continental, oceanic, and planetary volcanism. Geophys Monogr 100:438

Nelson CE, Jerram DA, Hobbs RW (2009) Flood basalt facies from borehole data: implications for prospectivity and volcanology in volcanic rifted margins. Pet Geosci 15:313–324

Pan Y, Wang ZX, Pan M (2014) Redefined distribution of the Permian volcanic rocks in the Tarim Basin: based on logging and seismic data. Appl Mech Mater 448-453:3723–3727

Peate IU, Larsen M, Lesher CE (2003) The transition from sedimentation to flood volcanism in the Kangerlussuaq Basin, East Greenland: basaltic pyroclastic volcanismduring initial Palaeogene continental break-up. J Geol Soc 160:759–772

Peate IU, Baker JA, Al-Kadas M, Al-Subbary A, Knight KB, Riisager P, Thirlwall MF, Peate DW, Renne PR, Menzies MA (2005) Volcanic stratigraphy of large-volume silicic pyroclastic eruptions during Oligocene Afro-Arabian flood volcanism in Yemen. Bull Volcanol 68:135–156

Pirajno F (2000) Ore deposits and mantle plumes. Academic Publication, Kluwer, p. 556

Planke S (1994) Geophysical response of flood basalts from analysis of wire line logs: ocean drilling program site 642, Vøring volcanic margin. J Geophys Res Solid Earth 99:9279–9296

Planke S, Cerney B, Nilsen O (1999) Alteration effects on petrophysical properties of subaerial flood basalts: site 990, Southeast Greenland margin. Proc Ocean Drill Program Sci Results 163:17–28

Pu RH, Dang XH, Xu J, Guo Q, Yi HJ (2011) Permian division and correlation and distribution of volcanic rocks of Tarim Basin. Acta Petrol Sin 27(1):166–180 in Chinese with English abstract

Pu RH, Zhang YL, Luo JL (2012) Seismic reflection, distribution, and potentialtrap of Permian volcanic rocks in the Tahe field. J Earth Sci 23(4):421–430

Reichow MK, Pringle MS, Al'Mukhamedov AI, Allen MB, Andreichev VL, Buslov MM, Davies CE, Fedoseev GS, Fitton JG, Inger S, Medvedev AY, Mitchell C, Puchkov VN, Safonova IY, Scott RA, Saunders AD (2009) The timing and extent of the eruption of the Siberian traps large igneous province: implications for the end-Permian environmental crisis. Earth Planet Sci Lett 277:9–20

Ren JY, Zhang JX, Yang HZ, Hu DS, Li P, Zhang YP (2011) Analysis of fault systems in the Central uplift, Tarim Basin. Acta Petrol Sin 27(1):219–230 in Chinese with English abstract

Tian W, Campbell IH, Allen CM, Guan P, Pan WQ, Chen MM, Yu HJ, Zhu WP (2010) The Tarim picrite–basalt–rhyolite suite, a Permian flood basalt from Northwest China with contrasting rhyolites produced by fractional crystallization and anatexis. Contrib Mineral Petrol 160:407–425

Wang HJ, Chi WL, Liu WZ, Cheng RH, Shan XL, Ren YG (2003) Volcanic facies of the Songliao Basin: classification, characteristics and reservoir significance. J Jilin Univ (Earth Sci Ed) 33(4): 449–456 in Chinese

Wu GY, Li YJ, Liu YL, Zhao Y, Li H (2012a) Petrochemistry and regional tectonic implications of Permian-early Triassic volcanic rocks in the Tabel rise, Tarim Basin. Mineral Petrol 32(4):21–30 in Chinese with English abstract

Wu GH, Yang HJ, Qu TL, Li HW, Luo CH, Li BL (2012b) The fault system characteristics and its controlling roles on marine carbonate hydrocarbon in the central uplift. Acta Petrol Sin 28(3):793–805 in Chinese with English abstract

Xinjiang Bureau of Geology and Mineral Resources (1993) Regional geology of theXinjiang Uygur autonomous region. Geology Publishing House, Beijing in Chinese

Xu YG, Chung SL, Jahn BM, Wu GY (2001) Petrologic and geochemical constraints on the petrogenesis of Permian-Triassic Emeishanflood basalts in southwestern China. Lithos 58:145–168

Xu YG, Wei X, Luo ZY, Liu HQ, Cao J (2014) The Early Permian Tarim large Igneous Province: main characteristics and a plume incubation model. Lithos 204:20–35

Yan L, Ling M, Pan WQ (2014) Distribution characteristics of Permian igneous rock in Tarim Basin—based on the high-precision aeromagnetic data. Prog Geophys 29(4):1843–1848 in Chinese with English abstract

Yang HF, Chen HL, Dong CW, Jia CZ, Wang ZG (1996) The discovery of Permian syenite inside Tarim Basin and its geodynamic significance. Geochimica 25(2):121–128 in Chinese with English abstract

Yang HF, Chen HL, Dong CW, Jia CZ, Wang ZG (1997) The discovery of Permian Basite zone inside Tarim Basin and its geodynamic significance. Geochimica 26(6):77–87 in Chinese with English abstract

Yang SF, Chen HL, Ji DW, Li Zl, Dong CW, Jia CZ, Wei GQ (2005) Geological process of early to middle Permian Magamtism in Tarim Basin and its geodynamic significance. Geol J China Univ 11(4):504–511 in Chinese with English abstract

Yang SF, Li ZL, Chen HL, Xiao WJ, Yu X, Lin XB, Shi XG (2006) Discovery of a Permian quartz syenitic porphyritic dyke from the Tarim Basin and its tectonic implications. Acta Petrol Sin 22:1405–1412 in Chinese with English abstract

Yu X, Yang SF, Chen HL, Chen ZQ, Li ZL (2011) Permian flood basalts from the Tarim Basin, Northwest China: SHRIMP zircon U–Pb dating and geochemical characteristics. Gondwana Res 20:485–497

Zhang SB, Gao QQ (1992) Stratigraphical paleontology from Sinian to Permian in the Tarim Basin. Petroleum Industry Press, Beijing, pp. 31–61 in Chinese

Zhang W, Guan P, Qi YM, Tian W, Feng F, Jian X, Wang YR (2014) Spatial distribution and main controlling factors of Permian volcanic rocks in Manxi-Awati area in the Tarim basin. Nat Gas Geosci 25: 79–90 in Chinese with English abstract

Zhao WZ, Shan WJ, Hu SY, Pan WQ, Zheng JF, Qiao ZF (2012) Types and distributional features of CambrianOrdovician dolostone reservoirs in Tarim Basin, northwestern China. Acta Petrol Sin 28(3): 758–768

Zhou MF, Malpas J, Song X, Kennedy AK, Robinson PT, Sun M, Lesher M, Keays RR (2002) A temporal link between the Emeishan large igneous province (SW China) and the end-Guadalupian mass extinction. Earth Planet Sci Lett 196:113–122

Zhou MF, Zhao JH, Jiang CY, Gao CF, Wang W, Yang SH (2009) OIB-like, heterogeneous mantle sources of Permian basaltic magmatism in the western Tarim Basin, NW China: implications for a possible Permian large igneous province. Lithos 113:583–594